Editor:
Supon, Ananta
Chiang Mai University, Thailand

Article history:
Received: June 2, 2021;
Revised: December 18, 2021;
Accepted: December 23, 2021;
https://doi.org/10.12982/CMUJNS.2022.021

Corresponding author:
Yusril Yusuf,
E-mail: yusril@ugm.ac.id

Research article

Hydroxyapatite based on Abalone Mussel Shells Coating on Titanium Alloy using Electrophoretic Deposition Dip Coating as a Bone Implant Candidate

Nicholas Adi Kristianto, Mona Sari, and Yusril Yusuf*

Department of Physics, Faculty of Mathematics and Natural Science, Universitas Gadjah Mada, Yogyakarta 55281, Indonesia

Abstract In this study, hydroxyapatite (HA) from abalone mussel shells (*Haliotis asinina*) is synthesized using the precipitation method with a stirring time of 30 min and a calcination temperature of 1000°C. HA was used for coating Ti alloy using the electrophoretic deposition dip coating (EP2D) method. The coating applied three variations, including the DC voltages variation of 25 V and 50 V, the withdrawal speeds of 0.1 mm/s, 0.5 mm/s, 1 mm/s, and the calcination temperatures of 750°C and 950°C. Energy dispersive X-Ray spectroscopy (EDS) revealed the Ca/P molar ratio of HA was 1.63, which is close to the stoichiometric ratio of HA at 1.67. The distance between the crystal planes of the HA was 2.81Å. This result also is relative to the crystal plane of the HA at 2.88Å. The EP2D process and the calcination temperature treatment will remove the B-type carbonate apatite phase, so the purity of the HA layer is higher. SEM results show that the HA layer formed was more homogeneous and thicker at the DC voltage of 50 V and the withdrawal velocity of 0.1 mm/s. At this voltage and velocity, minor cracking and agglomeration were produced. The density of the HA layer was higher with increasing calcination temperature and DC voltages.

Keywords: Hydroxyapatite, Titanium Alloy, Coating, Electrophoretic Deposition Dip Coating

Funding: The authors are grateful for the research funding provided by the Ministry of Education, Culture, Research, and Technology, the Republic of Indonesia.

Citation: Kristianto, N.A., Sari, M., and Yusril Yusuf, Y. 2022. Hydroxyapatite based on abalone mussel shells coating on titanium alloy using electrophoretic deposition dip coating as a bone implant candidate. CMU J. Nat. Sci. 21(2): e2022021.

INTRODUCTION

Bone is an organ with a complex and rigid structure, which makes up the human skeleton. Bones have the primary function of supporting the body, attaching muscle tissue to movement, and protecting various vital organs such as the brain, spinal cord, heart, and lungs (Kriswanto et al., 2020). Bones also have the function of reducing pressure. In addition, bone is also the dynamic, highly vascularized tissue that is formed from the composite of 70% mineral (mostly nanoscale HA crystals) and 30% organics (including collagen, glycoproteins, proteoglycans, and sialoproteins) by dry weight (Palmer et al., 2008).

For several years, there has been an increased demand for the replacement of bones or hard tissue damaged from various factors, such as osteoarthritis (inflammation in the joints of bone), osteoporosis (weakening of the bones), dentistry, war-related injuries, and traffic accidents (Singh et al., 2020; Sari et al., 2021). Nowadays, in Indonesia, bone implants are imported from other countries in the form of cemented Total Hip Replacement (THR) with a stem component inserted into the femur, which is made of titanium (Ti) alloy (Aminatun et al., 2015), but with increasing numbers of patients requiring bone replacements, there is a need for biomaterials that can be used to regenerate skeletal tissue (Singh et al., 2020; Syafaat and Yusuf, 2018; Kriswanto et al., 2020).

The use of metal biomaterial in the medical world has begun to be widely applied in the last twenty years. About 70% – 80% of implanted devices in the medical field are made of metal biomaterials. Metal biomaterials play an important role in fracture fixation, bone repair, and failed tissue (Harun et al., 2018). Metal biomaterials used explicitly for bone implants are Ti alloys, stainless steel, magnesium-based alloys, and cobalt-chromium alloys (Ananth et al., 2013; Aminatun et al., 2015; Singh et al., 2020). These metals have different characteristics, such as Young's modulus value, hardness, compressive strength, and so on. Ti and its alloys have become the most popular biomaterials for orthopedic and dental implants (Bartmanski et al., 2017). Ti alloys have proven relevant for their excellent corrosion resistance, appropriate mechanical properties, attractive biocompatibility, non-toxicity, perfect antibacterial character, and moderate elastic modulus (Singh et al., 2020; Aminatun et al., 2015).

The treatment for bone damage is to use metals, such as 316L stainless steel (316L SS), to replace damaged bones. However, this treatment creates problems due to the low level of biocompatibility of the metal, which causes pain and bruising in the surrounding tissue (Mulya et al., 2016). The 316L SS devices can also result in galvanic corrosion, crevices, and dangerous Cl and Fe ions release into tissues. Therefore, because these surfaces are not bioactive, they must be modified using osteoconductive material, such as bioceramics, including hydroxyapatite (HA; $(Ca_{10}(PO_4)_6(OH)_2)$ from the calcium phosphate family. HA's advantages are its porous, bioactive, non-corrosive, and wear-resistant properties. Currently, HA is deposited as a coating on metal coating materials to help suppress the release of harmful metallic ions (Singh et al., 2020). Accordingly, HA works as a bioceramic with excellent biological characteristics facilitating bone repair and reconstruction (Permatasari et al., 2019). However, the mechanical properties of HA are too weak to apply in load applications, so a combination of the substantial mechanical properties of the metal and the biocompatible property of HA is required. This combination can develop for bone implant applications (Hamidi et al., 2017).

A variety of techniques for synthesizing HA have been developed, such as the sol-gel procedure (Bakan et al., 2013; Peng et al., 2015), precipitation from an aqueous solution (Sari and Yusuf, 2018; Latocha et al., 2019; Gecim et al., 2021), hydrothermal (Jokic et al., 2011; Wu et al., 2013), and solid-state reactions (Wu et al., 2018). In this study, the precipitation method was selected based on specific considerations. Most HA synthesis approaches do not require any organic solvent, making it low-cost; this is also a simple process with high throughput (87%), making the method suitable for industrial production (Sari et al., 2021).

HA made by chemical synthesis is called synthetic HA. Synthetic HA can be obtained from synthetic or natural calcium-rich sources (Sari and Yusuf, 2018). Such raw materials include cow bones, fish bones, cuttlefish, and mussel shells (Sari et al., 2021). In the previous studies (Permatasari et al., 2019; Sari et al., 2021), abalone mussel shells

(*Haliotis asinina*) from Indonesia have been used as the natural compound for HA synthesis, as they consist of 90–95% calcium carbonate (Permatasari et al. 2021; Sari et al., 2021).

A variety of methods for the coating process on metal surfaces has also been developed, including dip coating (Aminatun et al., 2015), electrophoretic deposition (EPD) (Patel et al., 2015; Patel et al., 2016; Bartmanski et al., 2017; Patel et al., 2019; Kriswanto et al., 2020; Singh et al., 2020), sol-gel coating (Ahmadi and Afshar, 2021; Baladi et al., 2021), magnetron sputtering (Surmenev et al., 2021), and plasma spraying (Heiman et al., 2016; Singh et al., 2020). Among these, dip coating and EPD are the easiest; however, the EPD method has a greater chance of cracking due to manual withdrawal of the coating. Cracking in the layer dramatically affects the characteristics when implanted in the body (Kriswanto et al., 2020). In addition, the coating process using the dip-coating method requires more time (Aminatun et al., 2015). Therefore, combining the two approaches to impact controlling surface morphology, layer thickness, free cracking, and forming a homogeneous layer relatively quickly is necessary. Combining the two methods produces an electrophoretic deposition dip coating (EP2D). Magnetron sputtering and plasma spraying can be used for the coating process for advanced coating methods. Plasma spraying methods have the advantages of being fast, easy to control, economically advantageous, and, in their processing technology, coat almost any substrate with materials having a defined congruent melting point (Surmenev et al., 2021). Furthermore, magneton sputtering is widely used in vacuum technology for the deposition of various materials (Heimann et al., 2016).

Electrophoretic deposition dip coater combines a series of dip coater devices and EPD tools integrated on the computer (Sari et al., 2021). The difference between the EPD and EP2D processes lies in the coating process. EPD only uses an electric field without a substrate withdrawal process; meanwhile, the EP2D uses an electric field and a substrate withdrawal process.

HA was synthesized via precipitation using calcium carbonate ($CaCO_3$) from abalone mussel shells in the present study. In previous research (Sari et al., 2021), HA has been fabricated with the stirring time of HA solutions at 60 min and calcination temperature at 1000°C. In the present study, HA is synthesized via the precipitation method with a stirring time of 30 min and a calcination temperature at 1000°C. The characteristics of HA were observed, including its effect on crystallinity, Ca/P mol ratio, and functional groups of HA samples. HA was used to coat Ti alloy using the (EP2D) method developed by the author. The coating applied three variations, including DC voltages of 25 and 50 V, withdrawal velocities of 0.1, 0.5, and 1 mm/s, and calcination temperatures of 750 and 950°C. The physicochemical properties of HA/Ti coatings were characterized using scanning electron microscopy energy-dispersive X-ray spectroscopy (SEM-EDS) and X-ray diffractometer (XRD). The mechanical properties of HA/Ti coating were analyzed through compressive strength using Universal Testing Machine (UTM).

MATERIAL AND METHODS

Materials

The abalone mussel shells used as a source of calcium carbonate ($CaCO_3$) were taken from Bali, Indonesia (Permatasari et al., 2019; Sari et al., 2021). The precursors of diammonium hydrogen phosphate ($[NH_4]_2\ HPO_4$) and ammonium hydroxide (NH_4OH) 25% solution were purchased from Merck (USA). Ethanol 96% solution was obtained from Material Physics and Electronics Laboratory, Universitas Gadjah Mada, Yogyakarta, Indonesia. Ti plate (ASTM B265-GR.1) was purchased from NET ARTIDAYA as Engineering and Industrial Support Company Bekasi, Indonesia.

Synthesis of HA

The CaO and HA were fabricated during prior research, so the present study used those samples (Sari et al., 2021). In the present study, HA is synthesized via the precipitation method with a stirring time of 30 min and a calcination temperature at 1000°C.

Coating procedure for HA/Ti

Preparation of substrate for coating procedure

The substrate used was Ti alloy, cut to dimensions of 10 × 20 mm and a thickness of 0.5 mm. All substrate samples were sanded with 1500 grit sandpaper and soaked in acetone solution for one night to remove adhered dirt.

Preparation of HA solution

An amount of 0.4 gr HA was dissolved in 40 mL ethanol 96%. HA/ethanol solution was stirred with a magnetic stirrer for 60 min at a temperature of 60°C.

Coatings and calcination processes for HA/Ti

Coatings of HA/Ti were applied using EP2D, with two titanium substrates used as cathode and anode. The substrate for HA/Ti was put into HA/ethanol and was stirred with a magnetic stirrer with the DC source voltages of 25 and 50 V. The EPD process was carried out with an immersion time of 15 min. The two substrates were withdrawn from the HA/ethanol solution at the withdrawal velocities of 0.1, 0.5, and 1 mm/s, controlled by a stepper motor via a computer. The HA/Ti was dried at room temperature before calcinating at 750 and 950°C for 3 h using a furnace.

Characterization of HA particles and HA/Ti coating

Morphology, particle size distribution, thickness, and composition analysis

The morphology of the HA and the thickness of HA/Ti coating were determined by SEM-EDS (Joel JSM-6510LA-1400, Japan). The EDS included in the SEM performance was used to determine the compositions of the HA powders. These results were used to calculate the molar ratio of Ca/P in the HA powders. The particle size distribution of the HA was calculated based on the measurements of 100 randomly selected particles using ImageJ software version 2006 (National Institutes of Health (NIH), Bethesda, MD, USA) (Sari et al., 2021).

Crystallographic analysis

The crystallographic properties of HA from abalone mussel shells and HA/Ti coating were characterized by XRD (PAN analytical Type X'Pert Pro, Japan). The XRD data were recorded in the range of 2θ:10–80° using Cu–Kα radiation at λ=0.154 nm (Sari et al., 2021). The crystallographic properties were obtained from XRD results, which were analyzed using OriginPro software version 2018 (OriginLab Corporation, Northampton, MA) and MATLAB software version 2015 (MathWorks Inc, MIT, USA). The analysis of crystallographic properties, including the lattice parameters and crystallite size in HA/Ti samples, took the highest peak of each sample. This highest peak for the XRD pattern shows the high crystallinity of HA/Ti. It was one of the characteristics of HA as a bioceramic for coating with Ti alloy.

Fourier transform infrared spectroscopy (FTIR) analysis

FTIR (Thermo Nicolet iS10, Japan) was conducted to determine the functional groups of HA. The FTIR instrument was operated in the range of 400–4000 cm^{-1} (Sari et al., 2021).

Mechanical test and its statistical analysis

Mechanical test analysis through compressive strength parameters used the universal testing machine (TN20MD, Controlab, Paris, France). One-way analysis of variance (ANOVA) was used to analyze the influence of calcination temperature on compressive strength of HA/Ti coatings, adhered by Tukey's test, with P <0.05 considered statistically significant (Sari et al., 2021).

RESULTS

Physicochemical analysis of HA

The physicochemical properties of HA were characterized through SEM, XRD, and 200 FTIR, as shown in Figure 1. The synthesized HA had a small agglomerate shape with sizes below 5 μm (Figure 1A). As shown in Figure 1B, the HA particles had an average particle

grain size of 0.41 ± 0.01μm with the same percentage distribution of the sample size at 97.56% (calculated from 100 randomly chosen particles). The synthesized HA exhibited a Ca/P molar ratio of 1.63, which is close to the stoichiometric ratio of HA at 1.67 (Figure 1C). The XRD pattern of the HA made from abalone mussel shells is shown in Figure 1D. The synthesized HA peaked at 31.8° with an hkl index close to 211. These results agreed with data from the Joint Crystal Powder Diffraction Standard (JCPDS) No.09-0432. The crystallite size and microstrain, and X-ray density of the synthesized HA were (44.62 ± 4.81) nm, 0.00283, and 10.55 g/cm^3, respectively. As shown in Figure 1E, the synthesized HA exhibited the functional group of HA. The HA exhibited the stretching mode of OH^- at 3571 cm^{-1} and the bending modes of stretching v(P-O) mode of PO_4^{3-} at 963, 1016, and 1086 cm^{-1}, respectively. HA exhibited the functional group of CO_3^{2-} only at 1479 cm^{-1}.

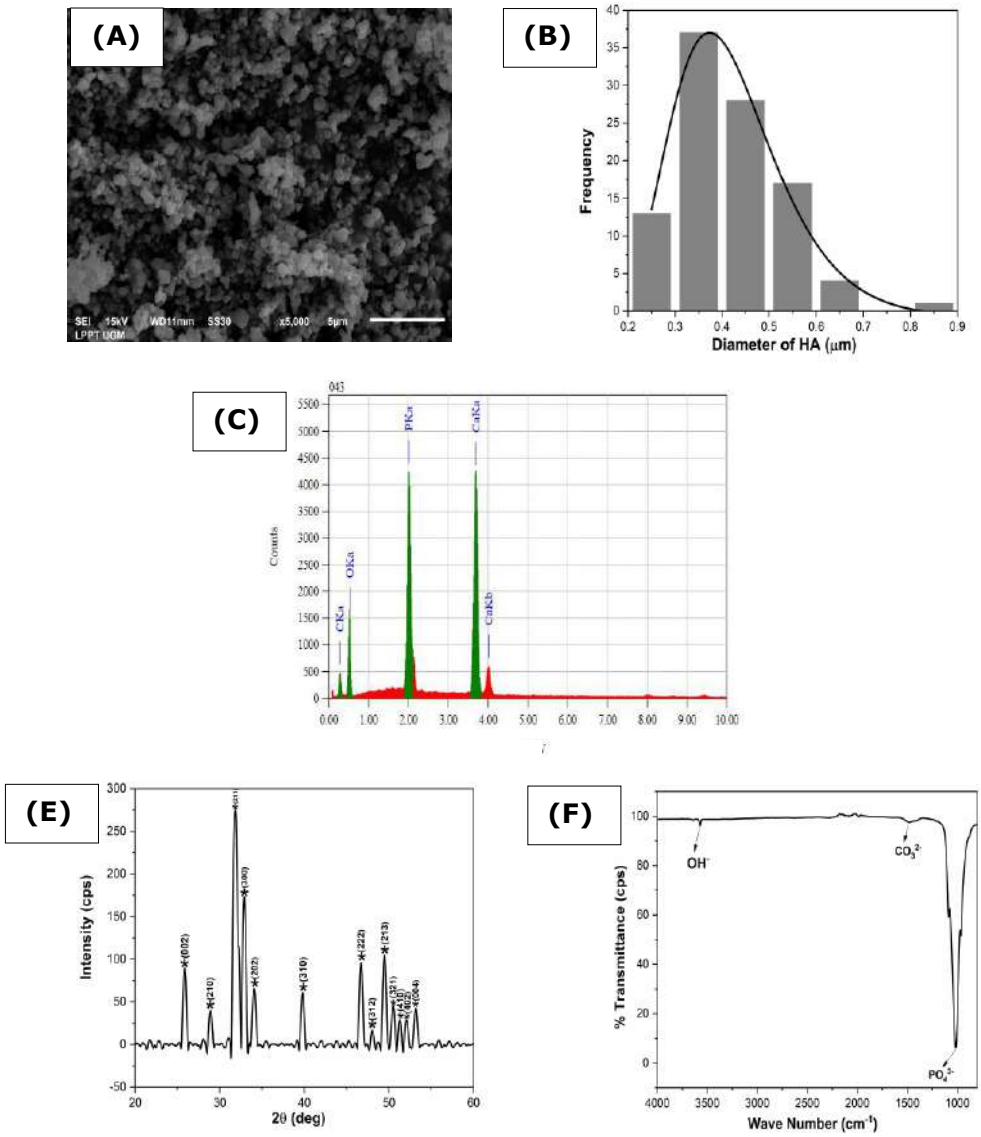

Figure 1. Physicochemical analysis of hydroxyapatite (A) morphology, (B) particle size distribution, (C)EDS analysis, (D)FTIR spectra, and (E)XRD pattern.

Electrophoretic deposition dip coating (EP2D) of HA/Ti coating

Thickness analysis by SEM

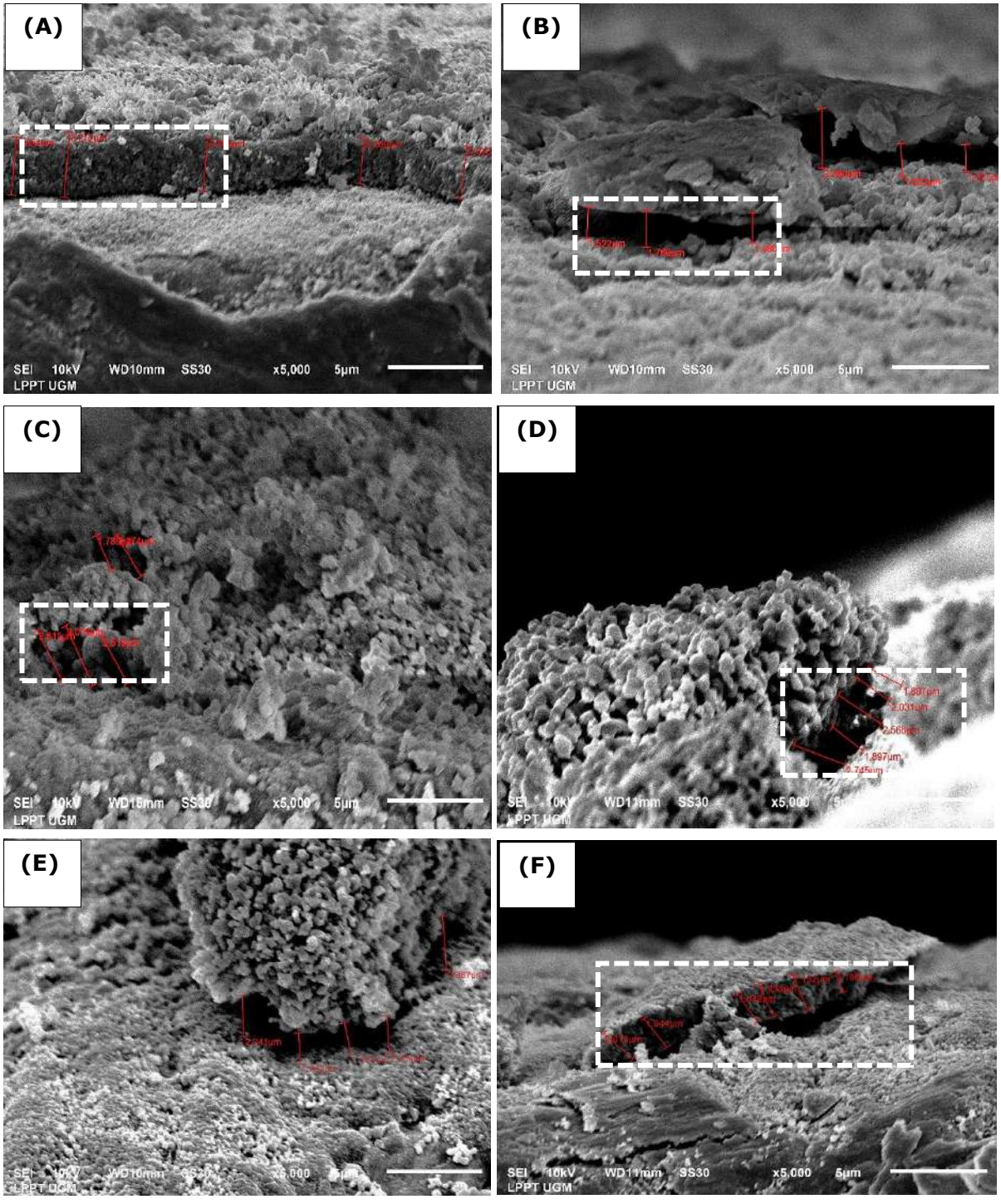

Figure 2. Cross-section of HA/Ti coating with variations of the withdrawal velocities, DC voltages, and calcination temperature of 750°C (A) 0.1 mm/s; 25V, (B) 0.1 mm/s; 50V, (C) 0.5 mm/s; 25V, (D) 0.5 mm/s; 50V, (E) 1 mm/s; 25V, and (F) 1 mm/s; 50V.
(The white dotted line indicates a cross-section of HA/Ti coating).

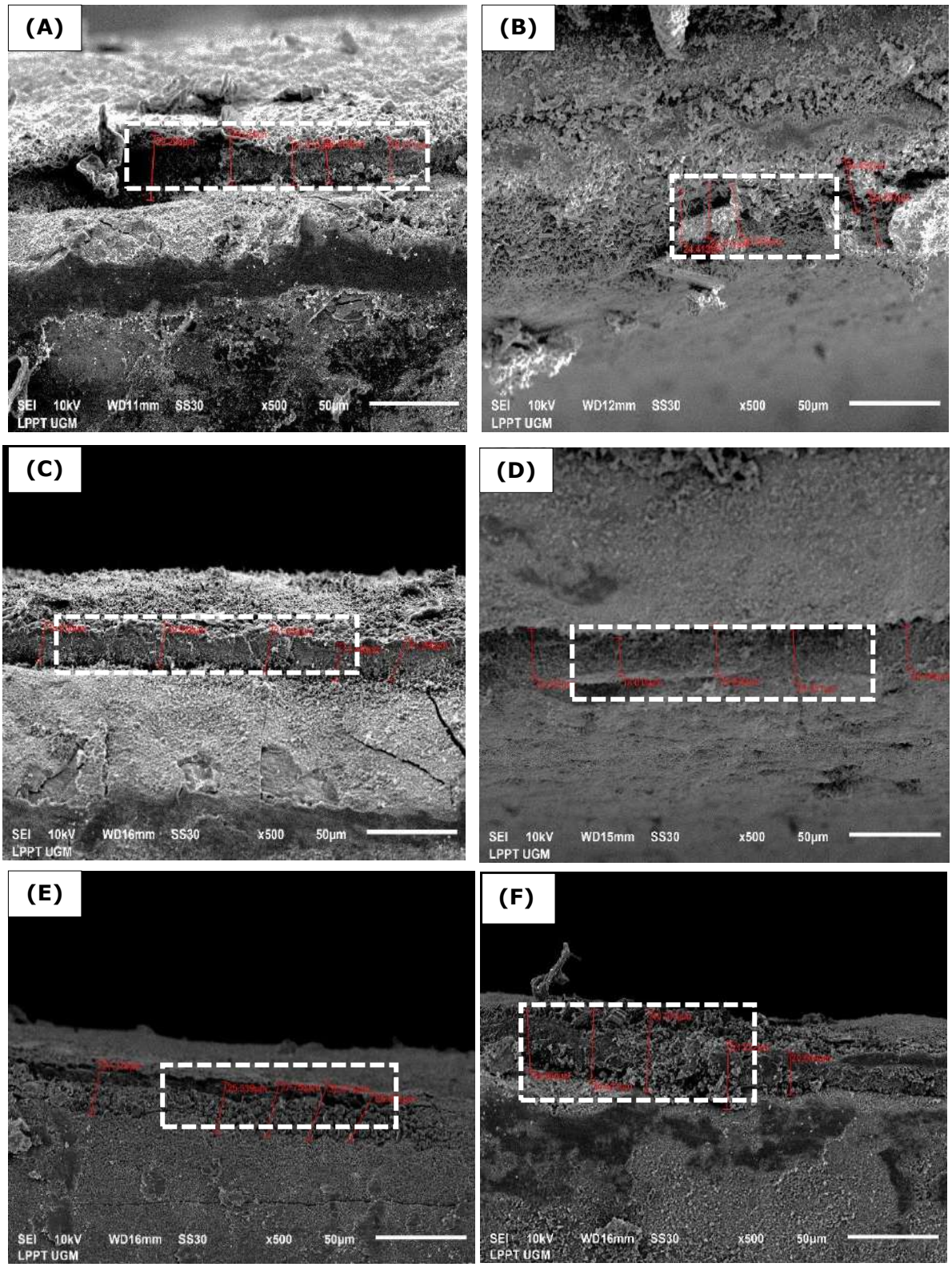

Figure 3. Cross-section of HA/Ti coating with variations of the withdrawal velocities, DC voltages, and calcination temperature of 950°C (A) 0.1 mm/s; 25V, (B) 0.1 mm/s; 50V, (C) 0.5 mm/s; 25V, (D) 0.5 mm/s; 50V, (E) 1 mm/s; 25V, and (F) 1 mm/s; 50V.
(The white dotted line indicates a cross-section of HA/Ti coating).

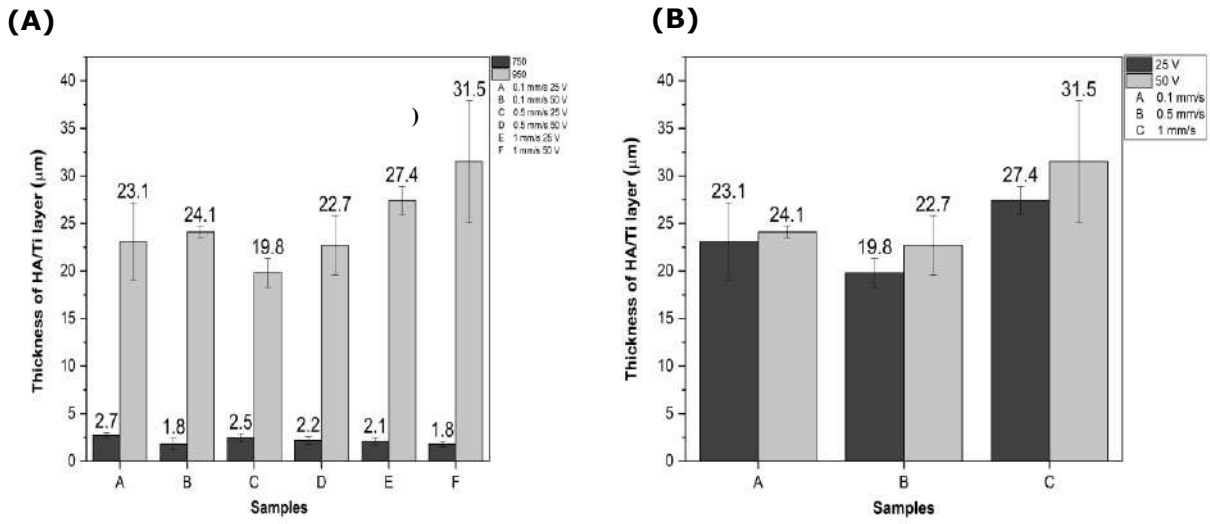

Figure 4. (A) Effect of calcination temperatures on the thickness of HA/Ti layer and (B) effect of DC voltages on the thickness of HA/Ti layer.

As shown in Figures 2 and 3, the HA/Ti layer with a calcination temperature of 950°C is thicker than that of a calcination temperature of 750°C, because the formation of the HA/Ti layer at a temperature of 950°C is more than the HA/Ti layer at a calcination temperature of 750°C. The variation in withdrawal velocity and DC voltage of the EPD process can increase the HA/Ti layer (Bartmanski et al., 2017). Based on Figures 2 and 3, the faster withdrawal during the EPD process will produce a thinner layer, while the higher EPD voltages will make the formed layer thicker.

As shown in Figure 4 (A and B), at a DC voltage of 50 V, the HA/Ti layer formed is larger than the HA/Ti layer at a DC voltage of 25V because the electrostatic force is more extensive. Thus, it pushes the HA particles in suspension, commonly called the particle deposition process, to move faster (Kriswanto et al., 2020). Based on these data, the thickness value for all samples was about 1.80–31.5 μm

XRD analysis

The XRD pattern of the HA layer on Ti alloy for DC voltages of 25 and 50 V, the withdrawal velocities of 0.1, 0.5, and 1 mm/s, and the calcination temperatures of 750 and 950℃ are shown in Figures 5 and 6. The X-ray diffraction pattern of the CHA/Ti coating was compared with the characteristics of Ti (JCPDS No.89-5009) and HA (JCPDS No.09-0432). As shown in Figures 5 and 6, the peaks of the XRD patterns in Figure 5 are sharper with higher intensity. In addition, there is a shift in the peaks in Figures 5 and 6 compared to the standard reference. This happens because of the strain on the crystal lattice, showing a more uniform strain (Figure 6). Thus, there is a shift in the central diffraction angles from the sample to the value of the smaller diffraction angle (Zak et al., 2011).

As shown in Table 1, the best results were obtained for the HA/Ti sample with the calcination temperature of 950 ℃, the withdrawal velocity of 0.1 mm/s, and the DC voltage of 50 V with the highest density. Because of its high density, the layer has a small porosity. Thus, it is not easily penetrated by water or other liquids. The presence of a voltage difference causes a higher density value. In this case, the crystal size of the HA/Ti layer is about 16 nm.

Table 1. Crystallography Properties of HA/Ti coating.

Samples	Lattice parameter (nm)		Density (gr/cm^3)	Crystallite size (nm)
	a=b	c		
750 °C, 0,1 mm/s, 25 V	9.37	6.73	3.27	16.23 ± 2.04
750 °C, 0,1 mm/s, 50 V	9.22	6.73	3.38	16.26 ± 2.06
750 °C, 0,5 mm/s, 25 V	9.27	6.63	3.39	16.46 ± 2.03
750 °C, 0,5 mm/s, 50 V	9.27	6.76	3.32	16.37 ± 2.02
750 °C, 1 mm/s, 25 V	9.48	6.89	3.12	16.33 ± 2.08
750 °C, 1 mm/s, 50 V	9.27	6.73	3.34	16.43 ± 2.02
950 °C, 0,1 mm/s, 25 V	9.32	6.75	3.29	16.40 ± 2.12
950 °C, 0,1 mm/s, 50 V	9.12	6.78	3.42	16.38 ± 2.20
950 °C, 0,5 mm/s, 25 V	9.27	6.73	3.34	16.39 ± 2.16
950 °C, 0,5 mm/s, 50 V	9.12	6.97	3.40	16.39 ± 2.02
950 °C, 1 mm/s, 25 V	9.32	6.78	3.28	16.50 ± 2.18
950 °C, 1 mm/s, 50 V	9.12	6.83	3.39	16.53 ± 2.03

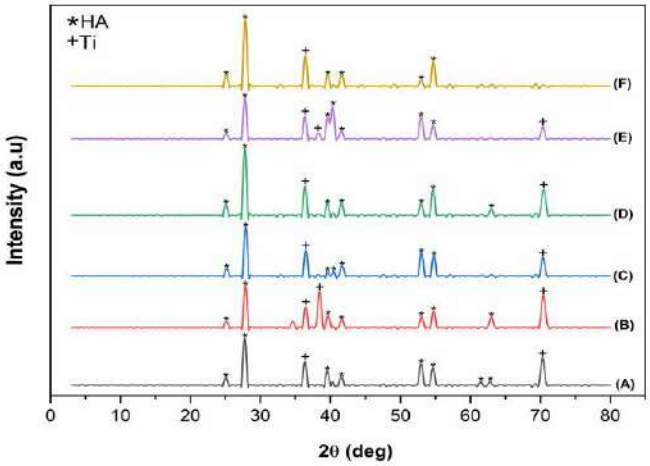

Figure 5. XRD pattern of HA/Ti coating with calcination temperature of 750°C (A) 0.1 mm/s; 25 V, (B) 0.5 mm/s; 25 V, (C) 1 mm/s; 25 V, (D) 0.1 mm/s; 50 V, (E) 0.5 mm/s; 50 V, and (F) 1 mm/s; 50 V.

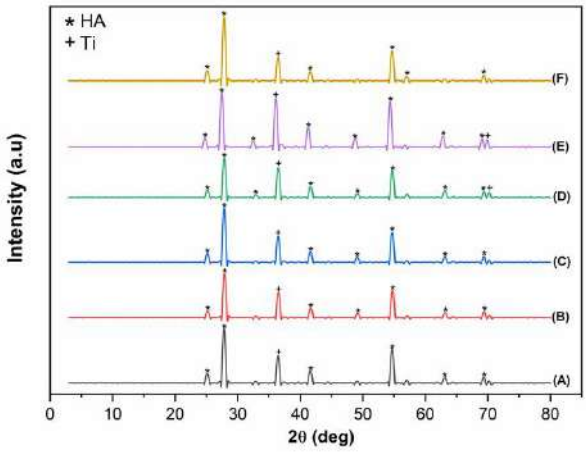

Figure 6. XRD pattern of HA/Ti coating with calcination temperature of 950°C (A) 0.1 mm/s; 25 V, (B) 0.5 mm/s; 25 V, (C) 1 mm/s; 25 V, (D) 0.1 mm/s; 50 V, (E) 0.5 mm/s; 50 V, and (F) 1 mm/s; 50 V.

Compressive Strength analysis

Based on physicochemical properties consisting of thickness analysis and crystallographic properties, HA/Ti coatings with DC voltage of 50 V and withdrawal of 0.1 mm/s have the best results. Therefore, mechanical testing through compressive strength analysis was done for these samples with calcination temperatures of 750°C and 950°C. As shown in Figure 7, calcination temperature influenced the mechanical properties of HA/Ti coatings (Sari et al., 2021). The compressive strength increased along with increasing the calcination temperature. According to ANOVA with Tukey test to determine the effect of calcination temperature on the compressive strength value, the *P*-value was 0.64 ($P > 0.05$). These results show no significant difference in the average compressive strength value in the two groups.

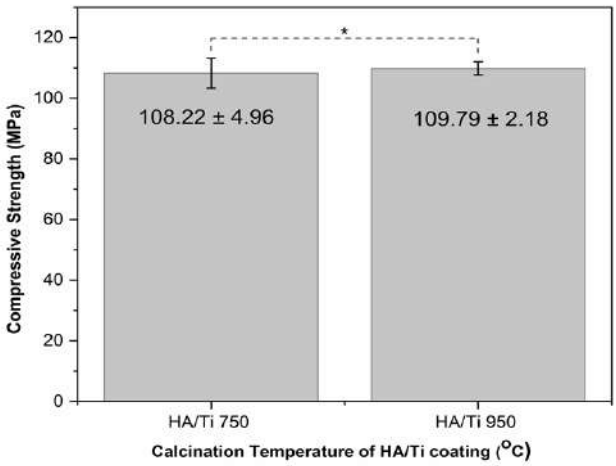

Figure 7. The average compressive strength value of HA/Ti coating with calcination temperatures of 750°C and 950°C (*: *P* > 0.05).

DISCUSSION

Physicochemical analysis of HA

The physicochemical properties of HA were analyzed by SEM, XRD, and FTIR results, as shown in Figure 1. As shown in Figure 1 (A), the morphology of synthesized HA resembled granules with uniform grains. The SEM results showed that synthesizing HA using the precipitation method produced a fine grain of uniform size (Sari et al., 2021). The distance between the crystal planes of the HA was determined using the Scherrer equation to be 2.81Å, as shown in XRD pattern analysis (Figure 1D). This result is close to the crystal plane of the HA at 2.88Å, making it appropriate by international standards (ISO 13779-3, ISO 13175-3) for HA implant (Sari et al., 2021; Gross et al., 1998). The existence of CO_3^{2-} groups in the FTIR spectra (Figure 1E) was due to calcium oxide's reaction with carbon dioxide in free air during synthesis. However, CO_3^{2-} groups may have existed in the abalone mussel shells before synthesis. Carbon dioxide came into contact with the distilled water solvent in this reaction and released CO_3^{2-} into the crystal lattice of the HA. The existence of CO_3^{2-} groups is common because they occur naturally in human bones (Sari et al., 2021).

Electrophoretic deposition dip coating (EP2D) of HA/Ti coating

In the EPD process, positively charged particles move toward the cathode due to the influence of the electric field, generating an electrostatic force (Besra and Liu, 2007). The form layer is deposited on the cathode, called cathodic electrophoretic deposition. The formation of this layer cannot be separated from the adhesion force that is the source of the bond between the surface of the Ti alloy substrate and the HA. This adhesion force

causes a bond between the hydrogen atoms of the sample and the substrate. Adhesion is considered the bond strength, which also implies the capacity of an adhesive or coating to stick to the surface and subsequently to bond the two surfaces together (Kriswanto et al., 2020).

The variations of DC voltages, withdrawal velocities, and calcination temperature affect the HA/Ti layer thickness, as shown in Figures 2–4. The faster the withdrawal during the EPD process will produce a thinner layer because it results in the deposition of formed particles experience release conditions. Thus, the resulting binding energy value is lower than the value of the withdrawal kinetic energy. The binding energy between the coating and the substrate will be more incredible, along with the drying and calcination processes after the EPD process. The higher the EPD voltages, the layer formed will be thicker because the higher the DC voltages will speed up the deposition time during the EPD process. This process will cause the influence of the electrostatic force to become stronger.

The thickness obtained (Figures 2–4) was less than 50 μm, while the thickness parameters required for coating were about 50–200 μm (Sánchez-Salcedo et al., 2008). If the coating result is less than 50 μm, the body will absorb the body around the HA/Ti implanted in the body. Thus, the HA/Ti layer composition parameters need to be improved for further study.

The B-type apatite content previously present in HA was not detected in the layer because applying a higher calcination temperature would decompose the B-type apatite, thereby increasing the purity of the HA in the layer (Kriswanto et al., 2020). Calcination temperature variation will also affect the shape of the HA particles in the titanium plate substrate. The calcination temperature of 950°C also showed that the HA was more even and more regular. This occurs due to the crystallization process of the nanomaterial with increasing calcination temperature (Youness et al., 2017).

The variations of the DC voltage, the withdrawal velocity, and the calcination temperature did not affect the crystallite size. The crystallite sizes obtained were close to one another, as shown in Figures 5 and 6 and Table 1. However, the lattice parameters of the HA/Ti coating experienced a change in the a and c lattice parameters of the samples. Changes in lattice parameters occurred due to the calcination process during the sample densification process (Permatasari et al., 2019; Sari et al., 2021).

Mechanical properties were influenced by surface morphology and coating composition (Sari et al., 2021). The HA/Ti coating with a calcination temperature of 950°C exhibited better compressive strength because of better densification (Youness et al., 2017). The analysis of surface charge (Zeta-Potential) and the degradation of the coatings in the phosphate buffer solution (PBS) will be characterized for further research.

CONCLUSION

This study presents a successful synthesis of HA based on abalone mussel shells with a molar ratio of Ca/P of 1.63, which is close to the stoichiometric ratio of HA at 1.67. The synthesized HA formed the same phase as HA, as confirmed through FTIR and XRD. The synthesized HA was used for the coating of Ti alloy using the EP2D method. The coating applied three variations, including the DC voltages of 25 and 50 V, the withdrawal velocities of 0.1, 0.5, and 1 mm/s, and the calcination temperatures of 750 and 950°C. These variations affect the thickness and crystallographic properties of the HA/Ti layer. The faster of the withdrawal velocities during the EPD process will produce a thinner layer, and the higher of the EPD voltage will create a thicker layer. Because the thickness obtained was less than 50 μm, the HA/Ti layer composition parameters need to be improved for further study. The calcination temperature of 950°C also showed that the HA was more regular. The best results were obtained by applying the calcination temperature of 950°C, the withdrawal speed of 0.1 mm/s, and the DC voltage of 50 V. This is supported by compressive strength analysis.

ACKNOWLEDGEMENTS

The authors are immensely grateful to the Ministry of Education, Culture, Research, and Technology, the Republic of Indonesia, for supporting this research. The authors acknowledge the use of the facilities and the technical assistance of the Material Physics and Electronics Laboratory and the Integrated Laboratory for Research and Testing staff at the Universitas Gadjah Mada, Indonesia.

AUTHOR CONTRIBUTIONS

Nicholas Adi Kristianto was involved in the study design, fabricated, characterized the HA/Ti coatings processes, performed the related analysis, interpreted the results, and drafted the manuscript. Mona Sari was involved in the study design, fabricated, characterized the HA from abalone mussel shells, performed the related analysis of HA, interpreted the results, and drafted and revised the manuscript. Yusril Yusuf contributed to the conception and study design, performed the corresponding analysis of HA and HA/Ti coatings and the interpretation of the results, drafted the manuscript, and revised the manuscript. All authors have read and approved the final manuscript.

CONFLICT OF INTEREST

The authors declare that they hold no competing interests.

REFERENCES

Ahmadi, R., and A. Afshar. 2021. *In vitro* study: Bond strength, electrochemical and biocompatibility evaluations of TiO_2/Al_2O_3 reinforced hydroxyapatite sol-gel coatings on 316L SS. Surface and Coatings Technology. 405: 126594.

Aminatun, Apsari, R., Yusuf , Y., and Suhariningsih. 2015. Synthesis and characterization of hydroxyapatite layer on cobalt alloys through dip coating method as a prosthetic bone implant candidate. Journal of Optoelectronics and Biomedical Materials. 7: 11–18.

Ananth, K.P., Suganya, S., Mangalaraj, D., Ferreira, J.M.F., and Balamurugan, A. 2013. Electrophoretic bilayer deposition of zirconia and reinforced bioglass system on Ti6Al4V for implant applications : An in vitro investigation. Materials Science and Engineering: C. 33: 4160–4166.

Bakan, F., Laçin, O., and Sarac, H. 2013. A novel low temperature sol-gel synthesis process for thermally stable nano crystalline hydroxyapatite. Powder Technology. 233: 295–302.

Baladi, J., Oh, T.H., and Sethuraman, M.G. 2021. Effects of pH on inhibitor-doped hybrid protective sol À gel coatings on the copper electrode surface. Journal of the Taiwan Institute of Chemical Engineers. 119: 259–268.

Bartmanski, M., Cieslik, B., Glodowska, J., Kalka, P., Pawlowski, L., Pieper, M., and Zielinski, A. 2017. Electrophoretic deposition (EPD) of nanohydroxyapatite-nanosilver coatings on Ti13Zr13Nb alloy. Ceramics International. 43: 11820–11829.

Besra, L., and Liu, M. 2007. A review on fundamentals and applications of electrophoretic deposition (EPD). Progress in Materials Science. 51: 51–61.

Gecim, G., Donmez, S., and Erkoc, E. 2021. Calcium deficient hydroxyapatite by precipitation : Continuous process by vortex reactor and semi-batch synthesis. Ceramics International. 47: 1917–1928.

Gross, K.A., Berndt, C.C., Stephens, P., and Dinnebier, R. 1998. Oxyapatite in hydroxyapatite coatings. Journal of Material Science. 3: 3985–3991.

Hadidi, M., Bigham, A., Saebnoori, E., Hassanzadeh-Tabrizi, S.A., Rahmati, S., Alizadeh Z.M., Nasirian, V., and Rafienia, M. 2017. Electrophoretic-deposited hydroxyapatite-copper nanocomposite as an antibacterial coating for biomedical applications. Surface Coating Technology. 321: 171–179.

Heimann, R.B. 2016. Plasma-sprayed hydroxyapatite-based coatings: Chemical, mechanical, microstructural, and biomedical properties. Journal of Thermal Spray Technology. 25: 827-850.

Harun, W.S.W., Asri, R.I.M., Alias, J., Zulki, F.H., Kadirgama, K., Ghani, S.A.C., and Shariffuddin, J.H.M. 2018. A comprehensive review of hydroxyapatite-based coatings adhesion on metallic biomaterials. Ceramics International. 44: 1250–1268.

Jokic, B., Mitric, M., Radmilovic, V., Drmanic, S., Petrovic, R., and Janackovic, D. 2011. Synthesis and characterization of monetite and hydroxyapatite whiskers obtained by a hydrothermal method. Ceramics International. 37: 167–173.

Kriswanto, M., Khairurrijal, M., Wajong, D.L.J., Kadarismanto, T.M., and Yusuf, Y. 2020. Stainless steel 316 L metal coating with capiz shell hydroxyapatite using electrophoretic deposition method as bone implant candidate. Key Engineering Materials. 840: 336–344.

Latocha, J., Wojasinski, M., Sobieszuk, P., Gierlotka, S., and Ciach T. 2019. Impact of morphology-in fl uencing factors in lecithin-based hydroxyapatite precipitation. Ceramics International. 45: 21220–21227.

Mulya, N., Fadli, A., and Amri, A. 2016. Pengaruh penambahan hidroksiapatit dan waktu pencelupan terhadap pelapisan logam *stainless steel* 316L dengan metode dip coating. Jom FTEKNIK. 3: 1–7.

Palmer, L.C., Newcomb, C.J., Kaltz, S.R., Spoerke, E.D., and Stupp, S.I. 2008. Biomimetic systems for hydroxyapatite mineralization inspired by bone and enamel. Chemical Reviews. 108: 4754–4783.

Patel, K.D., Mahapatra, C., Jin, G.Z., Singh, R.K., and Kim, H.W. 2015. Biocompatible mesoporous nanotubular structured surface to control cell behaviours and deliver bioactive molecules. ACS Applied Materials & Interfaces. 7: 26850–26859.

Patel, K.D., Singh, R.K., Mahapatra, C., Lee, E.J., and Kim, H.W. 2016. Nanohybrid electro-coatings with controlled drug delivery potential for bone regeneration. Journal of Biomedical Nanotechnology. 12: 1876–1889.

Patel, K.D., Buitrago, J.O., Parthiban, S.P., Lee, J.H., Singh, R.K ., Knowles J.C., and Kim, H.W. 2019. Combined effects of nanoroughness and ions produced by electrodeposition of mesoporus bioglass nanoparticle for bone regeneration. ACS Applied Bio Materials. 2: 5190–5203.

Patel, K.D., Singh, R.K., Lee, E.J., and Kim, H.W. 2016. Electrophoretic coatings of hydroxyapatite with various nanocrystal shapes. Materials Letters. 234: 148-154.

Peng, H., Wang, J., Shansan, Lv., Wen, J., and Chen, J. 2015. Synthesis and characterization of hydroxyapatite nanoparticles prepared by a high-gravity precipitation method. Ceramics International. 41: 14340–14349.

Permatasari, H.A., Supii, A.I, Suparta, G.B., and Yusuf, Y. 2019. Characteristics of abalone mussel shells (*Halioitis asinina*) with calcination temperature variations as a basic material for synthesis of carbonated hydroxyapatite. Key Engineering Materials. 818: 31–36.

Permatasari, H.A., Sari, M., Aminatun., Suciati, T., Dahlan, K., and Yusuf, Y. 2021. Nano-carbonated hydroxyapatite precipitation from abalone shell (Haliotis asinina) waste as the bioceramics candidate for bone tissue engineering. Nanomaterials and Nanotechnology. 11: 1–9.

Sánchez-Salcedo, S., Arcos, D., and Vallet-Regi, M. 2008. Upgrading calcium phosphate scaffolds for tissue engineering applications. Key Engineering Materials. 377: 19-42.

Sari, M., and Yusuf, Y. 2018. Synthesis and characterization of hydroxyapatite based on green mussel shells (*Perna viridis*) with calcination temperature variation using the precipitation method. International Journal of Nanoelectronics and Materials. 11: 357–370.

Sari, M., Hening, P., Chotimah, Ana, I.D., and Yusuf, Y. 2021. Bioceramic hydroxyapatite-based scaffold with a porous structure using honeycomb as a natural polymeric Porogen for bone tissue engineering. Biomaterials Research. 25: 1–13.

Sari, M., Hening, P., Chotimah, Ana, I.D., and Yusuf, Y. 2021. Porous structure of bioceramics carbonated hydroxyapatite-based honeycomb scaffold for bone tissue engineering. Materials Today Communication. 26: 102135.

Sari, M., Kristianto, N.A, Chotimah, Ana, I.D., and Yusuf, Y. 2021. Carbonated hydroxyapatite-based honeycomb scaffold coatings on a titanium alloy for bone implant application– Physicochemical and mechanical properties analysis. Coatings. 11: 1-18.

Singh, S., Singh, G., and Bala, N. 2020. Electrophoretic deposition of hydroxyapatite-iron oxide-chitosan composite coatings on Ti – 13Nb – 13Zr alloy for biomedical applications. Thin Solid Films. 697: 137801.

Surmenev, R.A., Ivanova, A.A., Epple, M., Pichugin V.F., and Surmeneva M.AG. 2021. Physical principles of radio-frequency magnetron sputter deposition of calcium-phosphate-based coating with tailored properties. Surface & Coatings Technology. 413: 127098.

Syafaat F.Y., and Yusuf, Y. 2018. Effect of Ca: P concentration and calcination temperature on hydroxyapatite (HAp) powders from quail eggshell (*Coturnix Coturnix*). International Journal of Nanoelectronics and Materials. 11: 51–58.

Wu, S., Tsou, H., Hsu, H., Hsu, S., Liou. S., and Ho W. 2013. A hydrothermal synthesis of eggshell and fruit waste extract to produce nanosized hydroxyapatite. Ceramics International. 39: 8183–8188.

Wu, S., Hsu, H., Hsu, S., Chang, Y., and Ho, W. 2018. Synthesis of hydroxyapatite from eggshell powders through ball milling and heat treatment. Journal of Asian Ceramic Societies. 4: 85–90.

Youness, R.A., Taha, M.A, and Ibrahim, M.A. Effect of sintering temperatures on the *in vitro* bioactivity, molecular structure and mechanical properties of titanium/carbonated hydroxyapatite nanobiocomposites. Journal of Molecular Structure. 1150: 188–195.

Zak, A.K., Majid, W.H.A., Abrishami, M.E, and Yousefi, R. 2011. X-ray analysis of ZnO nanoparticles by Williamson Hall and size strain plot methods. Solid State Sciences. 13: 251–256.

OPEN access freely available online
Chiang Mai University Journal of Natural Sciences [ISSN 16851994]
Chiang Mai University, Thailand
https://cmuj.cmu.ac.th